Photonic Crystal Fibers for Light Generation

Deniz Aydin[1,*], Steevy Cordette[1], and Camille-Sophie Brès[1]
[1]Photonic Systems Laboratory, Ecole Polytechnique Fédérale de Lausanne (EPFL), CH-1015 Lausanne, Switzerland
*Corresponding author: deniz.aydin@epfl.ch

Abstract: We study dispersion properties of photonic crystal fibers for their use in coherent light generation in visible wavelengths through optical parametric amplification. We use a simple 2D cross-sectional model of the holey fiber and solve for the guided modes. The models developed in this study of PCFs allow us to tailor the dispersion profile of PCFs using the geometric parameters of the fiber. We obtain phase-matching in the visible and infrared wavelengths. In addition, we extracted the dispersion profile of higher order modes which could be useful in further intermodal four-wave mixing studies.

Keywords: photonic crystal fibers, optical parametric amplifiers

1. Introduction

Optical parametric amplifiers (OPA) continue to garner interest for their ability to generate coherent light or amplify light in arbitrary wavelength regions. These devices are in contrast to traditional lasers where the emission wavelengths are determined by the electronic transitions available in the gain media. PCFs are of particular interest in such nonlinear optics applications because of the enhanced light confinement and the resultant high nonlinearity (γ) achievable with air-cladded designs. Additionally, the geometric parameters of the PCFs provide multiple degrees of freedom for dispersion engineering and allows for phase matching in arbitrary wavelength regimes. The ability to engineer the PCF waveguide dispersion coupled with the material choices available for fiber construction allows fine-tuning of the dispersion profile [1]. In turn, a flexible dispersion profile enables phase-matching in arbitrary wavelength regimes to take advantage of interesting nonlinear effects, such as four-wave mixing (FWM).

2. Governing Equations

In this section we detail the physics behind the four-wave mixing process, and we refer the interested reader to [2], [3] for detailed explanations of the phenomenon. This process is commonly described as the annihilation of two degenerate pump photons ($2\omega_p$) and the subsequent creation of the signal and idler photons (ω_s, ω_i), and is denoted $2\omega_p = \omega_s + \omega_i$ using conservation of energy. Importantly, we note that four-wave mixing is a process whose conversion efficiency is described by the phase matching requirement between the electromagnetic waves participating in this interaction: namely, the pump, signal and idler waves. For the undepleted pump case, and neglecting waveguide losses, we can define the idler gain due to four-wave mixing at point z along the length of the wave propagation as in Eq. (1):

$$G_i(z) = \left|\frac{\gamma P_0}{g}\sinh(gz)\right|^2 \tag{1}$$

$$G_s = G_i + 1 \tag{2}$$

And the signal gain is given as in Eq (2). In Eq (1) we have γ, the nonlinear coefficient of the waveguide and P_0, the initial pump power. We also see g, the parametric gain coefficient which is a function of the phase mismatch as described below:

$$g = \sqrt{\gamma {P_0}^2 - (\kappa/2)^2} \tag{3}$$

where κ is the total phase mismatch between the pump, idler and signal waves which has a contribution form the linear and non-linear phase mismatch terms (Eq(4)):

$$\kappa = \Delta\beta_L + 2\gamma P_0 \tag{4}$$

Where the linear phase mismatch term comes from the dispersion of the waveguide, and is expressed as:

$$\Delta\beta_L = \beta_2\Delta\omega^2 + \frac{\beta_4}{12}\Delta\omega^4 \quad (5)$$

Since we also know that dispersion of a waveguide is related to the propagation constants as in Eq (6).

$$D = \frac{d\beta_1}{d\lambda} = -\frac{\lambda}{c}\frac{d^2 n_{eff}}{d\lambda^2} \quad (6)$$

And we obtain the m-th propagation constant by taking the derivative of the propagation constant β with respect to the angular frequency as in Eq (7).

$$\beta_m = \frac{d^m\beta}{d\omega^m}_{\omega=\omega_0} \quad (7)$$

In order to determine the propagation constants to obtain the phase-matching conditions of the waveguide, we use COMSOL Multiphysics' Mode Analysis module to extract the effective refractive index and therefore the higher-order propagation constants. Mode Analysis solves the wave equation (Eq. (8)) in the 2D cross-section of the photonic crystal fiber:

$$\nabla \times \nabla \times \boldsymbol{E} - k_0^2\epsilon_r \mathbf{E} = \mathbf{0} \quad (8)$$

$$\epsilon_r = (n_{eff} - ik)^2 \quad (9)$$

Where in Eq. 8 we have the wave equation with the electric field E, wave-vector k_0 and relative permittivity of the material ε_r. We also have the relative permittivity expressed in terms of a real and a complex component in Eq. 9, where the real part represents the effective refractive index of the guided mode.

3. Methods and Model

As mentioned above, we solve the wave equation in the PCF cross-section. For the core-guided modes, such solid-core PCFs are effectively step-index fibers with an effective refractive index that can be determined from the wave equation and the auxiliary equations for the dielectric constant (Eq (8-9)). The fiber simulated is made of 20 mol. % GeO_2-doped silica core (illustrated red in Fig. 1) in silica matrix, with three rings of triangular lattice of air holes (r_{hole}= 1.4μm, Λ=3μm, r_{core}= 0.6μm).

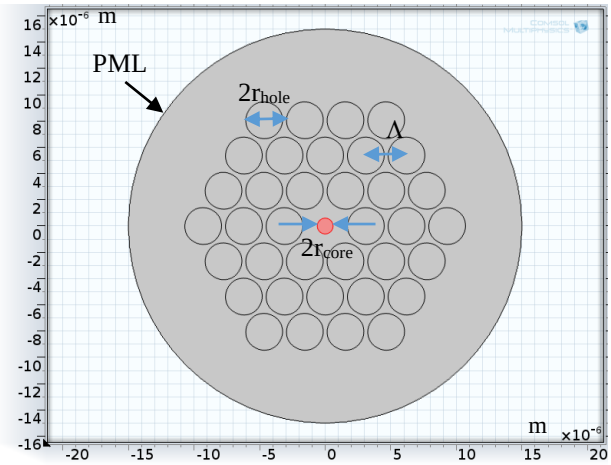

Figure 1. Transverse cross-section of the photonic crystal fiber used as the simulation domain.

The high air-filling fraction (d_{hole}/Λ ~0.93) enables strong confinement of the core-guided modes and thus increases the nonlinear coefficient, which is inversely proportional to the effective area (A_{eff}) of the mode

$$\gamma = \frac{n_2\omega}{cA_{eff}} \quad (10)$$

Where n_2, the nonlinear refractive index, a material-dependent property of the waveguide; ω the angular frequency of the propagating mode, c the usual speed of light. We have used the electromagnetic waves frequency domain to solve the wave equation under the perfectly matched layer boundary conditions applied

to the outer diameter of the PCF section. We note that it is also possible to use the perfect electric conductor for the boundary condition since for static models we can assume that the fields are zero at the boundary if the boundary is sufficiently far from the localized modes. This model includes no input electric field since, as mentioned, the problem is an electrostatic one. Finally, a parametric sweep of wavelengths is used to extract the dispersion profile of the waveguide on the wavelengths of operation, namely between 500nm and 2000nm with a 5nm resolution. For the fiber designs with larger core sizes used in the calculation of higher order mode dispersion profiles, we asked for ~100 modes to be found by the mode solver. This problem can be quite memory dependent due to both the complicated physical domain and the ensuing fine meshing, and the wide range of frequencies covered in by the parametric sweep. In order to reduce the time requirements, it is possible to use only half of the fiber with periodic boundary conditions.

We calculate A_{eff} in the COMSOL model by defining the integration operation bellow:

$$A_{eff} = \frac{(\int |E|^2 dA)^2}{\int |E|^4 dA} \tag{11}$$

The resultant effective area at 1μm is 3.5 μm^2 for the selected design, yielding a $\gamma \sim 50\ W^{-1}\ km^{-1}$.

4. Simulation Results

4.1 Dispersion Tuning

To tune the dispersion curves of PCFs we vary the air hole size, pitch, and the doped core size. In the below results, the doping concentration is fixed at 20 mol. %, which yields Δn = 30e-3, maximum achievable by our supplier. In order to achieve distant narrowband phase-matching in the visible and C-band regions we tailor the zero dispersion wavelength to around 1056nm.

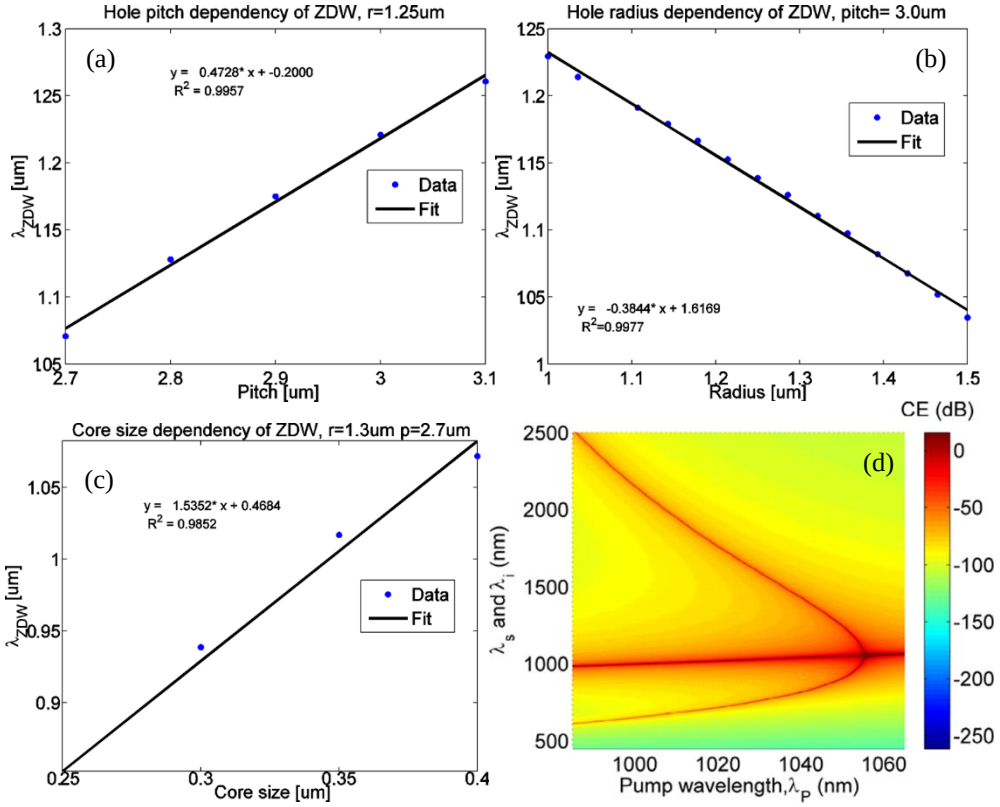

Figure 2. (a-c) Effect of PCF geometry on the zero-dispersion wavelength. Both hole-array pitch and the doped-core size have a directly linear relationship to the ZDW whereas the air hole radius is inversely proportional to the ZDW. Figure (d) shows the phase matching contours for the selected design.

Figure 2 we show the effect of tuning the PCF geometry on the zero-dispersion wavelength (λ_{ZDW}). In (a) we see that the effect of air hole pitch (hole-to-hole distance) is to linearly increase the λ_{ZDW} if all other parameters are fixed. Similarly in (c), we observe a linear relationship between the size of the GeO_2-doped core and the λ_{ZDW}. Conversely to these two examples, air hole radius is inversely proportional to the zero-dispersion crossing, as is expected from previous work ([4]). Notably the ratio of air hole diameter to pitch, often denoted the "air filling fraction" d/Λ, is inversely proportional to the zero-dispersion wavelength.

An important diagram is Figure 2 (d), which is the phase-matching curves for the selected PCF design with λ_{ZDW} = 1056nm. As seen from the plot this selection of the zero-dispersion location allows us to achieve narrowband phase matching over a wide range of visible and infrared frequencies simultaneously by pumping the nonlinear fiber in the normal dispersion regime. The red-coloured regions in the plot indicate the maximal gain wavelengths for a specific pump wavelength (λ_p).

4.2 Higher-order modes in PCF

Here we present an estimate of the number of modes that could be supported by a PCF with the given filling fraction using a previous work [5]. We estimate that based on the models from [5], [6] we could expect to see a V-number between 4 - 6 for a PCF with d/Λ~0.9 operating at 1μm(Figure 3). As such, we can assume that number of modes supported can be $M = V^2/4 = 4 – 9$ respectively for the two estimates.

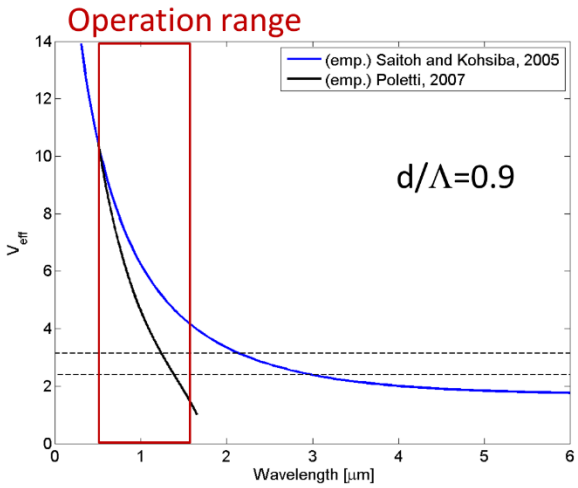

Figure 3. Estimate for the V-parameter of custom designed photonic crystal fiber. Each curve represents an estimate using different approaches.

We finally simulate higher order guided modes in the photonic crystal fibers in order to see the relative shift in dispersion between the various modes. As shown in Fig. 4 the TEM00 mode has the longest zero dispersion wavelength, and the subsequent higher order modes (TEM01* and TEM03 respectively) have shorter zero-dispersion wavelengths. While the dispersion profile for the higher order modes extends to above 1.5μm the fiber may not be multimode at these long wavelengths based on Figure 3 estimates of the cutoff wavelength. While different works cite V = 2.405 [7] and V=π [4] as cut-off values for PCF single-mode operation if we choose the worst-case scenario of the lower limit, we see cutoff wavelengths of about ~1.385μm and ~3μm. In the case that the fiber is experimentally found to be indeed multimode at the operation wavelengths, conversion efficiency might be sacrificed due to random inter-mode mixing as previously described in the literature [8]. However, achieving such short λ_{ZDW} for the sake of visible to C-band phase matching requires such extraordinarily high filling fractions, which come at the cost of multimode operation.

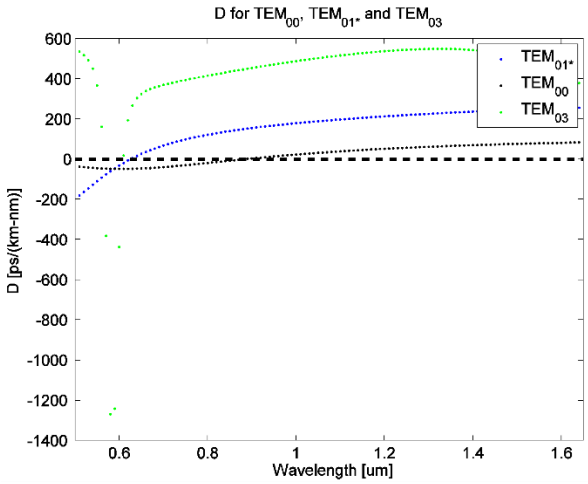

Figure 4. Dispersion of TEM00, TEM01 and TEM03 modes in a photonic crystal fiber.*

5. Conclusions

In this work, we simulated the dispersion properties of PCFs for narrowband phase-matching in the visible and C-bands. Computation of effective refractive index (n_{eff}), effective area (A_{eff}), visualization of guided modes allowed for the design of a suitable nonlinear fiber for phase matched four-wave mixing to be used in coherent light generation at visible wavelengths. Phase-matching in distant bands is made possible with the optimized design. Selected design accesses visible and C- and L-bands simultaneously for wavelength conversion into the visible using a signal at these telecom wavelengths and a pump around 1μm. PCFs with short ZDW are multimode in the visible wavelengths, which poses a risk to lose from conversion efficiency due to random linear intermode coupling.

6. References

[1] P. S. J. Russell, "Photonic-Crystal Fibers," vol. 24, no. 12, pp. 4729–4749, 2006.

[2] M. E. Marhic, *Fiber Optical Parametric Amplifiers, Oscillators and Related Devices*. publisherNameCambridge University Press, 2007.

[3] G. Agrawal, *Nonlinear Fiber Optics*. 2000.

[4] M. Nielsen and N. Mortensen, "Photonic crystal fiber design based on the V-parameter.," *Opt. Express*, vol. 11, no. 21, pp. 2762–2768, 2003.

[5] K. Saitoh and M. Koshiba, "Numerical modeling of photonic crystal fibers," *J. Light. Technol.*, vol. 23, no. 11, pp. 3580–3590, 2005.

[6] F. Poletti, "Direct and inverse design of microstructured optical fibres," 2007.

[7] M. Koshiba and K. Saitoh, "Applicability of classical optical fiber theories to holey fibers," vol. 29, no. 15, pp. 1739–1741, 2004.

[8] Y. Xiao, R.-J. Essiambre, M. Desgroseilliers, A. M. Tulino, R. Ryf, S. Mumtaz, and G. P. Agrawal, "Theory of intermodal four-wave mixing with random linear mode coupling in few-mode fibers," *Opt. Express*, vol. 22, no. 26, p. 32039, 2014.

7. Acknowledgements

None.